International Journal of Multiphase Flow 37 (2011) 1093–1098

Contents lists available at ScienceDirect

International Journal of Multiphase Flow

journal homepage: www.elsevier.com/locate/ijmulflow

Energy spectra and bubble velocity distributions in pseudo-turbulence: Numerical simulations vs. experiments

Ivo Roghair [a,*], Julián Martínez Mercado [b], Martin Van Sint Annaland [a], Hans Kuipers [a], Chao Sun [b], Detlef Lohse [b]

[a] Multiphase Reactors Group, Department of Chemical Engineering and Chemistry, Eindhoven University of Technology, P.O. Box 513, 5600 MB Eindhoven, The Netherlands
[b] Physics of Fluids Group, Faculty of Science and Technology, J.M. Burgers Centre for Fluid Dynamics and IMPACT Institute, University of Twente, P.O. Box 217, 7500 AE Enschede, The Netherlands

ARTICLE INFO

Article history:
Received 3 January 2011
Received in revised form 8 July 2011
Accepted 11 July 2011
Available online 20 July 2011

Keywords:
Bubbly flow
Front tracking
Pseudo-turbulence
Bubble velocity

ABSTRACT

Direct numerical simulations (DNS) are performed to study the behavior of a swarm of rising air bubbles in water, employing the front tracking method, which allows to handle finite-size bubbles. The swarms consist of monodisperse deformable 4 mm bubbles with a gas fraction of 5% and 15%. This paper focuses on the comparison of the liquid energy spectra and bubble velocity probability density functions (PDFs) with experimental data obtained by phase-sensitive constant-temperature anemometry (CTA) and three-dimensional particle tracking velocimetry (PTV), respectively.

The numerical simulations confirm that the spectra of the velocity fluctuations driven by the rising bubbles follow a power law with slope close to −3, supporting the idea that the dissipation of the bubble wake is the origin of this spectral scaling, as previously proposed by Lance and Bataille.

The computed PDFs of the bubble velocity show non-Gaussian features, as is also observed in the experiments. The agreement with experimental measurements is especially good in the peak region, whereas the tails of the experimental PDFs show more intermittency in comparison to the numerical results. This can be explained by the lack of large-scale flow structures in the simulations, and by the large difference in measurement time.

1. Introduction

Bubble columns are gas–liquid contacting devices frequently used in the (bio)chemical, and metallurgical industries. Detailed knowledge on the behavior and interaction of both phases is essential for a proper design and optimization, in which numerical modeling at different scales can play a crucial role (Deen et al., 2004). As bubbles rise through the liquid column, they induce liquid fluctuations which are referred to as pseudo-turbulence. A correct understanding of the pseudo-turbulence is critical for the simulation of bubbly flows, since it influences momentum, heat, and mass transfer rates.

The characteristics of these turbulent fluctuations in the liquid are reflected in the energy spectrum. It has been shown that the energy cascade of pseudo-turbulence behaves differently from homogeneous single-phase turbulence, and hence deserves special attention in large-scale models. Lance and Bataille (1991) studied bubbles rising through an imposed turbulent flow. They measured the energy spectrum of the fluctuations and found a power law scaling with a slope of about −8/3, in contrast to the classical −5/3 for homogeneous single-phase turbulence. They explained the change of the slope as a wake dissipation effect. Their scaling argument gives an exponent of −3, close to the experimentally found value. The value −3 has also been obtained by Risso (2011), arguing that the signals from the wake of the rising bubbles would be viewed as a sum of localized random bursts with statistically independent strength and size.

In contrast, in the numerical work on pseudo-turbulence by Mazzitelli and Lohse (2009) a slope of −5/3 of the energy spectrum was observed together with a stable inverse energy cascade, where the energy input occurs on the small scales (i.e. rising bubbles). Energy is then transferred to large scales, building up large-scale motion. However, in those simulations bubbles were approximated as point-like particles, thus disregarding finite-size effects and capillary phenomena. As Mazzitelli and Lohse (2009) mentioned in their paper, the "wrong" −5/3 scaling cannot be the signature of real (experimental) bubble columns.

Indeed, the experimental work of Martínez Mercado et al. (2010) found a scaling of the energy spectrum close to −3 for various gas fractions in the very dilute regime. These results were obtained by single-point measurements in flows with gas fractions

* Corresponding author. Tel.: + 31 40 247 3975; fax: + 31 40 247 5833.
E-mail address: i.roghair@tue.nl (I. Roghair).

0301-9322/$ - see front matter © 2011 Elsevier Ltd. All rights reserved.
doi:10.1016/j.ijmultiphaseflow.2011.07.004

ranging from $\alpha = 0.8$–2.2%, using a phase-sensitive CTA probe. Furthermore, in the work by Riboux et al. (2010) energy spectra were measured with PIV in the wake of a bubble swarm (because PIV measurements could *not* be done *within* the swarm due to the light reflection at the bubbles' interface). Their results confirmed a scaling close to -3 for length scales larger than the bubble diameter. For smaller length scales their measurements recovered the $-5/3$ slope. The scaling was independent of bubble diameter and bubble concentration. Numerically, Bunner and Tryggvason (2002b) computed the power spectrum for a swarm of ellipsoidal bubbles employing the front tracking method and found a slope of -3.6. They also observed a strong anisotropic flow, in contrast to Lance and Bataille (1991). They explained the difference by arguing that a large-scale convection pattern, induced by the bubbles, was present in the experiments.

The PDF of bubble velocities provide useful information for modeling force correlations used in bubbly flow simulations. Bunner and Tryggvason (2002b, 2003) and Esmaeeli and Tryggvason (2005) numerically obtained PDFs of the bubble velocity for non-deformable and deformable bubbles. For the case of non-deformable spherical bubbles, the PDFs have a Gaussian distribution whereas for ellipsoidal deformable bubbles the PDFs deviated from Gaussian at low void fractions, recovering Gaussianity only as the bubble density increases. Experimentally, PDFs of bubble velocity have been measured by Zenit et al. (2001) and Martínez Mercado et al. (2007). Their measurements were carried out using an intrusive technique and the number of data points used for the PDFs was not sufficient to determine a well defined distribution.

In this work, in an attempt to improve on the point-bubble simulations of Mazzitelli and Lohse (2009), we carry out DNS of bubble swarms with a Front Tracking model aiming at resolving the bubbles' wake. With this approach both finite-size and shape deformations (by tracking the bubbles' interface) can be taken into account. In this manner it will be possible to quantify whether bubble wake phenomena influence the energy spectrum scaling. We will provide a direct comparison of our numerical energy spectra and other statistical properties like PDFs of the bubble velocity with the experimental results by Martínez Mercado et al. (2010) and discuss the differences. Of particular interest are air bubbles in water. That implies that we use a density ratio of $\rho_g/\rho_l = O(1000)$ and a viscosity ratio of $\mu_g/\mu_l = O(100)$.

One of the strongest advantages of numerics is the non-intrusive access to velocities and velocity-derived quantities in the whole numerical domain. Besides that, the void fraction can be considerably larger as compared to experiments which rely on optical techniques, which are restricted to very dilute bubbly flows, such as PTV (Martínez Mercado et al., 2010) or laser doppler anemometry (LDA) (Risso and Ellingsen, 2002; Mudde et al., 1997). On the other hand, due to computational restrictions, the simulated domain sizes and times are much smaller than those typically used in experiments, leading to poor statistics in the simulations.

This paper starts with a short description of the Front Tracking model, including details on the data sampling by our numerical probes. Then results of energy spectra of the liquid fluctuations and bubble velocity distributions are presented and compared to experimental results. The last section summarizes and discusses the present work.

2. Numerical method

2.1. Front tracking

Direct numerical simulations are performed using a full three-dimensional Front Tracking model (based on the method by Unverdi and Tryggvason (1992) and Tryggvason et al. (2001)). Details on the actual implementation are given in Dijkhuizen et al. (2010b), while validation with experiments using single rising bubbles is given in van Sint Annaland et al. (2006) and Dijkhuizen et al. (2010a). Furthermore, we have favorably compared the velocity of a single rising bubble, with the results presented in Bunner and Tryggvason (2002a).

The model solves the incompressible Navier–Stokes Eq. (1) using a one-fluid formulation on a Eulerian grid using a source-term $\mathbf{F}_\sigma$ to account for the surface tension force at the interface:

$$\rho\frac{\partial \mathbf{u}}{\partial t} + \rho\nabla\cdot(\mathbf{uu}) = -\nabla p - \nabla\cdot\boldsymbol{\tau} + \rho\mathbf{g} + \mathbf{F}_\sigma, \tag{1}$$

$$\nabla\cdot\mathbf{u} = 0. \tag{2}$$

The equations are solved using a 2-step projection-correction method, firstly resolving the momentum equations with semi-implicit shear stress terms (projection), followed by a pressure-correction step. Both iterative approaches use an incomplete Cholesky conjugate gradient (ICCG) matrix solver on a single CPU.

The interface between the phases is tracked using Lagrangian marker points (control points). These control points are interconnected, forming a triangular mesh, from which the surface tension force $\mathbf{F}_\sigma$ can be calculated. This force is mapped back to the Eulerian grid at the location of the interface, using mass-weighing. After calculation of the flow field, the marker points are moved with the interpolated fluid flow, which eventually may result in edges of the triangular mesh varying in size. A remeshing procedure assures that the size of these edges is kept within predefined limits, e.g. by removing or adding marker points.

The flow field has periodic boundaries in all three directions. In order to prevent the system from energetically diverging due to the buoyancy force (see e.g. Calzavarini et al., 2006), the net average fluid flow velocity (volumetric flux) is subtracted from each velocity vector every time step.

2.2. Typical conditions

The bubbles are initially spherically shaped and placed randomly throughout the cubic uniform computational domain. The fluid flow velocity is set to zero. Our base-case is air-water (with a Morton number $\mathrm{Mo} = g\mu_l^4(\rho_l - \rho_g)/(\rho_l^2\sigma^3) = 2.5\times10^{-11}$). Table 1 shows the physical parameters for the air–water case. We adjust the size of the computational domain to obtain the desired void fraction. Using 20 Eulerian cells in a bubble diameter d_b ensures accurate results while keeping the computation time as short as possible—using $d_b = 4$ mm, the grid cell size is 2×10^{-4} m. A number of $N_b = 16$ bubbles are used. With this choice of N_b, our results are independent of the number of bubbles. This was checked by comparing bubble rise velocities in simulations varying N_b between 4 and 32. Moreover, Bunner and Tryggvason (2002a) mentioned that at least 12 bubbles should be used. The bubble Reynolds number $\mathrm{Re_b} = \rho_l u_b d_b/\mu_l$ is of order O(1000). The Eötvös number is $\mathrm{Eo} = g d_b^2(\rho_l - \rho_g)/\sigma = 2.15$.

The simulation time is 4 s and we use a time step of 5×10^{-5} s. In Dijkhuizen et al. (2010a), it was shown that using a time step of 10^{-4} s provides same averaged results as a time step of 10^{-5} s for a

Table 1
Physical properties for the air–water simulations.

Viscosity (gas phase) μ_g	1.8×10^{-5} (mPas)
Density (gas phase) ρ_g	1.25 (kg/m^3)
Viscosity (liquid phase) μ_l	0.001 (mPas)
Density (liquid phase) ρ_l	1000 (kg/m^3)
Surface tension coefficient σ	0.073 (N/m)
Gas fraction α	0.05–0.15 (–)

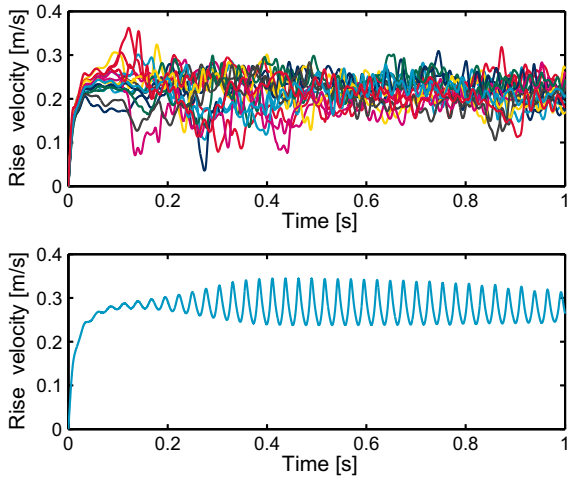

Fig. 1. The transient period of 4 mm bubbles in a swarm (top) is much smaller (less than 0.2 s) than that of a single rising bubble in an "infinite" liquid (bottom).

single rising bubble. Reducing the time step is done for stability purposes and not for accuracy.

2.3. Data acquisition

To exclude transient effects of the initially quiescent liquid and bubbles, the interval of 0.0–0.2 s is discarded for the analysis. In Fig. 1 it is shown that for bubbles in a swarm, the transient period is actually much shorter (less than 0.2 s) than for single rising bubbles in an infinite liquid. The bubbles in a swarm start to interact with each other very soon, whereas for a single rising bubble the transient lasts longer and its "wobbling" profile oscillates steadily only after 0.5 s. The bubble velocities are sampled each 1×10^{-4} s, as the velocity of the center-of-mass of the bubble, which is determined from the location of the marker points on the interface mesh.

For the energy spectra calculations numerical probes were used. These probes register the phase fraction and the fluid velocity vector in the computational cell at each time step (typically 5×10^{-5} s), providing a signal very similar to the signal from the experiments. Also, the size of the computational cells is comparable to the experimental probe. Hence, these probes are the numerical equivalent to the phase sensitive CTA as described in van den Berg et al. (2011) and Martínez Mercado et al. (2010). An array of $3 \times 3 \times 3$ probes was located throughout the computational domain.

Due to the staggered discretization of the velocity field, a linear interpolation from the cell edges was performed for the phase fraction and velocity at the cell center. Fig. 2 shows both a typical signal for the phase fraction and velocity from numerics and those obtained with a phase-sensitive CTA probe by Martínez Mercado et al. (2010).

There are some slight differences with the experimental probes, however. Because the velocity of both phases is defined on a single velocity field, the signal is continuous even when an interface crosses the probe. In addition, the phase is represented as a fraction (i.e. the gas fraction in the computational cell) instead of a binary phase indicator.

3. Energy spectra

For the calculation of the energy spectra of liquid fluctuations we follow the method described in Martínez Mercado et al. (2010). Since the numerical phase indicator is not binary as in

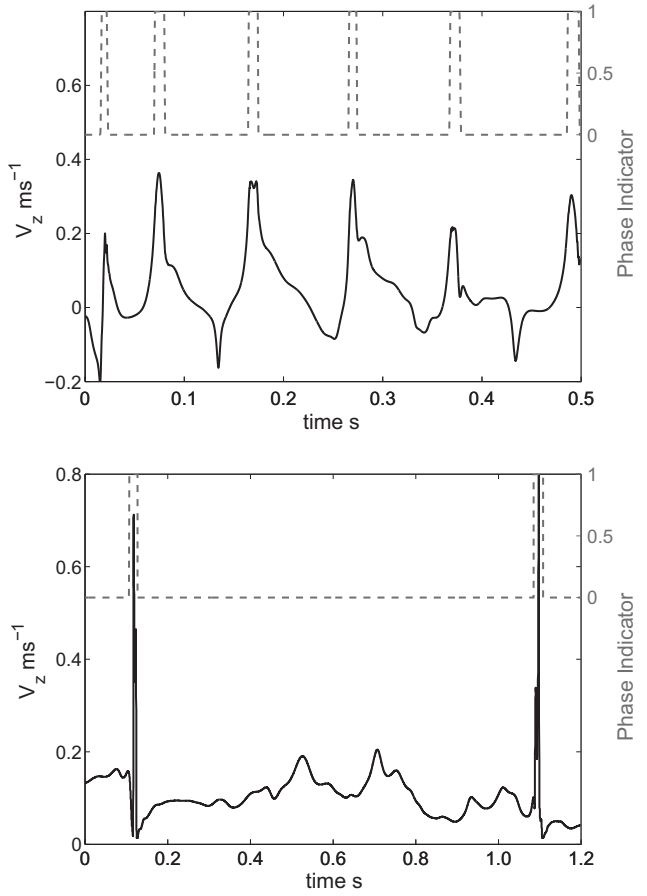

Fig. 2. Typical velocity and indicator function signals. The solid line shows the vertical fluid velocity, the dashed line the phase fraction (0: liquid, 1: bubble). Upper figure: single numerical probe for a low void fraction simulation. Lower figure: experimental phase-sensitive CTA probe. Note that the phase fraction of the simulation is twice as high as in the experiments.

the experimental data, we set it to zero if the cell contains only liquid. Therefore, we have a collection of segmented velocity signals in time for each numerical probe. For each probe we calculate the power spectrum density of the segments larger than 256 data points and average over all segments. Finally, an ensemble average over all the 27 probes is done to obtain the final power spectrum. Experimentally, in Martínez Mercado et al. (2010) the liquid velocity fluctuations were measured with a cylindrical hot-film probe with its axis oriented along the (horizontal) x direction. Hence, their spectra accounted for fluctuations in the y and z directions. For this reason, we also report the energy spectrum considering the fluctuations of these components of the velocity (E_{yz}), which give the same result as compared to E_{xz} as can be seen in Fig. 3. We stress the key role that the simulation time plays to achieve statistical convergence of the spectrum for all the numerical probes. If the simulation time is not long enough, each spectrum obtained from the numerical probes will depend strongly on its location. For an air–water system, we have found that at least 4 s of simulation time is needed. Fig. 4 shows the spectra of each of the 27 probes for a 4-second air–water simulation with $\alpha = 5\%$. All curves have the same behavior, reflecting the good convergence. We mention that we have also run simulations with more concentrated bubble swarms and with higher-viscosity liquids. Within 2 s of simulation time, full convergence of the spectra of the individual probes is not achieved for these cases.

We therefore focus on the fully converged case of the air–water simulation with $\alpha = 5\%$. Fig. 5 shows the averaged spectrum of all

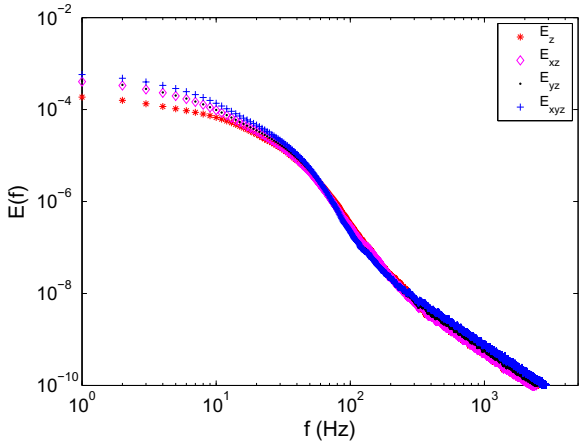

Fig. 3. The energy spectra calculated considering different components of the fluctuations are similar. Higher energies are obtained when more velocity components are taken into account.

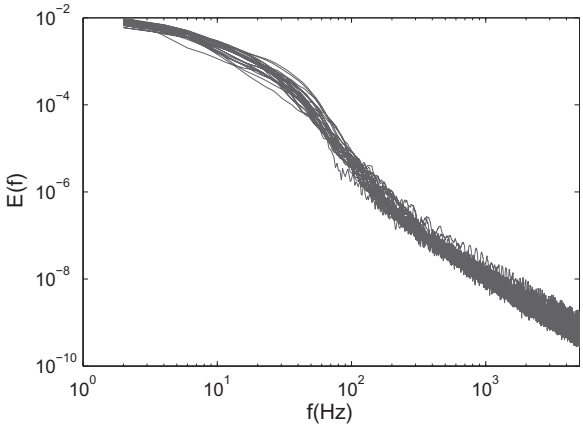

Fig. 4. The energy spectra of each of the 27 numerical probes of a 4 s air–water simulation with $\alpha = 5\%$. All the spectra show a well-converged similar behavior that is independent of the probe location. The spectra of half as long simulations do not show this good convergence yet, neither do simulations with increased viscosity.

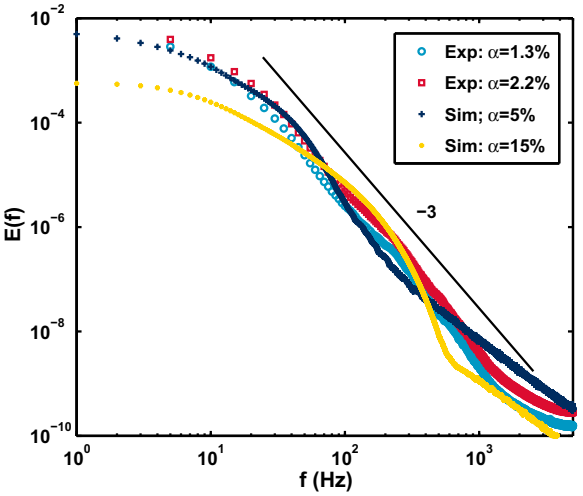

Fig. 5. The energy spectra of the simulation is compared to experimental results. For the simulation with $\alpha = 5\%$, a power law close to -3 is observed for nearly one decade starting for frequencies of about 20 Hz till 200 Hz. We also show the simulation case with $\alpha = 15\%$ and with 2 s simulation time, which is not yet fully converged.

27 numerical probes together with the experimental data by Martínez Mercado et al. (2010). The simulation shows a good agreement, having a slope close to -3 in the frequency range of 20–200 Hz. The scaling frequency range for the numerics is shorter as compared to the experimental case due to the difference in simulation and measurement time. Risso and Ellingsen (2002) pointed out that the power spectra are not influenced by α, based on their experimental findings. In spite of a shorter simulation time and the above discussed convergence problems, in Fig. 5 we also show the spectra for a case with $\alpha = 15\%$. Due to the smaller signal segments, caused by the smaller distance between the bubbles at higher gas loadings, the -3 scaling range shrinks to less than a decade.

4. Bubble velocity distribution

Fig. 6 shows the (logarithm of the) PDFs of the bubble velocity normalized by their standard deviation. As it is very difficult either in numerics to reduce α without exponentially increasing the required computation time or to increase α in experiments due to the optical restriction that PTV imposes for detecting single particles, for the experimental case we picked the most concentrated flow which could be measured using three-dimensional PTV in Martínez Mercado et al. (2010), namely $\alpha = 0.74\%$. For the numer-

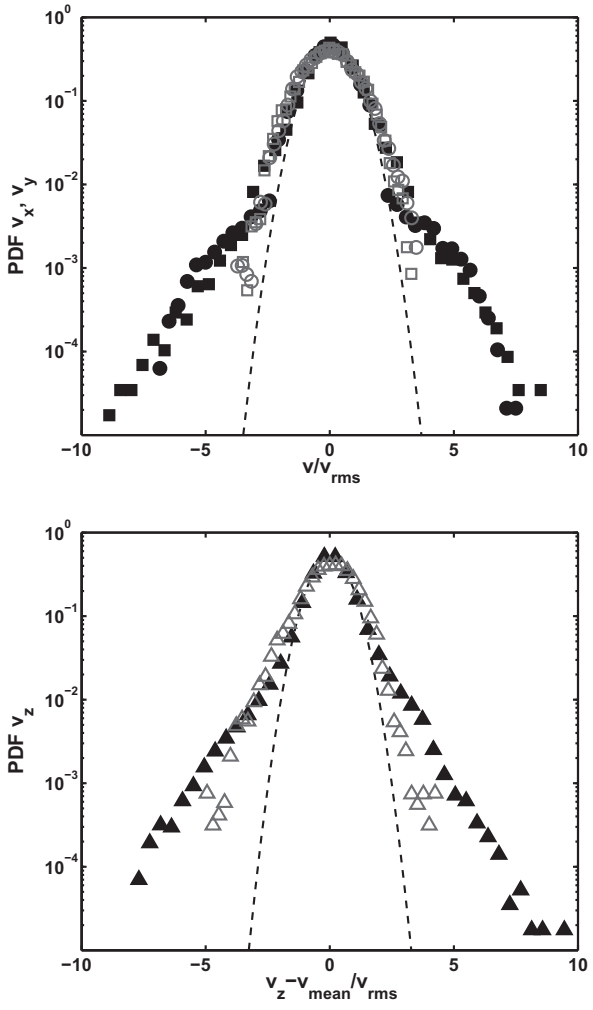

Fig. 6. Probability density functions of bubble velocity. Solid symbols represent simulations ($\alpha = 5\%$), open symbols experiments ($\alpha = 0.74\%$), dashed line represents a Gaussian distribution with the same mean and width as in experiments. The upper figure shows the horizontal velocity components. ○: v_x and □: v_y. The lower figure shows v_z.

ical simulations we picked $\alpha = 5\%$ instead, where (i) we have the best statistics and (ii) which still can be considered as dilute.

Fig. 6 shows the results for the horizontal and for the vertical components. In spite of the difference in bubble concentration, the PDFs agree reasonably well in the velocity range where we can numerically determine it. We point out that the central part of the PDFs are on top of each other and have a probability 1000 times higher than the events in the tails. Note that the measuring time in experiments is longer, so there is a larger chance of detecting the rare events leading to the pronounced tails of the PDFs. It is not possible to detect them numerically, due to CPU time limitations. In addition, large-scale structures do occur in the flow in the experimental water channel, which are not seen in our simulations due to the different boundary conditions. The deviation from Gaussianity can be observed in both cases, even in the central region, as the dashed line in Fig. 6 suggests. For a fair comparison of the flatness value, from the experimental results we have only selected velocities which are in the central part of the PDF, i.e. $-4 < (v - v_{\mathrm{mean}})/v_{\mathrm{rms}} < 4$, which results in a flatness of around 4–5 for the horizontal components and flatness around 5.5 for the vertical velocity. From numerics, at $\alpha = 5\%$ we get values around 3 for the horizontal components and 3.8 for the vertical component.

An investigation of the flatness as a function of the gas fraction using the numerical data shows that also for larger gas fractions $\alpha > 5\%$ the flatness of the z-component is higher than that of the horizontal components, which is consistent with the Gaussian case with flatness equals to 3.

5. Discussion and conclusions

Results from Front Tracking DNS of a swarm of deformable air bubbles in water have been analyzed. We have compared the power spectrum of bubble induced turbulence (pseudo-turbulence) and bubble velocity distributions with experimental data of a bubble column.

We have shown that the liquid energy spectrum follows a power law with a slope close to -3, which agrees with the experimental results in the frequency range 20–200 Hz. Our finding gives additional support to the idea that this particular power law scaling in pseudo-turbulence is related to the wake of the bubbles. Whether the actual mechanism is dissipiation or transfer should be further investigated. Mazzitelli and Lohse (2009) performed pseudo-turbulence simulations with point-particle bubbles, they found the classical Kolmogorov $-5/3$ power law, as the point-particle approach cannot resolve the wakes of the bubbles. Experiments by Roig and de Tournemine (2007) and Risso et al. (2008), and theoretical arguments by Lance and Bataille (1991) and Risso (2011) have also indicated the importance of bubbles' wake phenomena. Hence, the finite-size leading to wake formation accounts for the pseudo-turbulence -3 spectrum measured by Lance and Bataille (1991) and Martínez Mercado et al. (2010).

The bubble velocity PDFs show a good agreement with experiments. Both experimental and numerical data deviate from a Gaussian distribution. Experimental data show larger tails than the numerical results due to the relatively short simulation time (because of the computational cost), but also because of the periodic boundary conditions used in the model. When using periodic boundary conditions, the possibility of occurrence of large scale patterns and rare velocity events is reduced. We do however observe a similar trend concerning the flatness of the PDFs: the vertical velocity distributions have a higher flatness than the horizontal components. We expect that if modifying the boundary conditions and longer simulation times were possible, the incidental high velocities in the tails of the distributions will also occur in the numerical simulations.

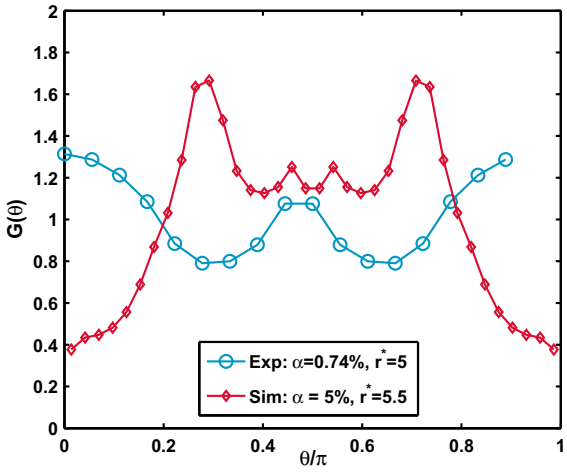

Fig. 7. The angular pair correlation function $G(\theta)$ does not show a good agreement between simulations and experiments especially on the vertical clustering, which is due to the domain boundary conditions.

Another consequence of the periodic boundary conditions in the numerics is that the spatial structure of the bubbles cannot be correctly captured. We have analyzed clustering effects on the numerical data by calculating the angular pair correlation function $G(\theta)$, the probability density function of the angle between the vertical axis and the vector connecting the centroids of two bubbles. In Fig. 7 numerical and experimental results are shown (details on $G(\theta)$ can be found in Martínez Mercado et al., 2010), where the numerical simulation contains a gas fraction of 5% which is the closest to the gas hold-ups used in experiments. However, the radius used in the simulations (normalized by the bubble diameter) is slightly larger due to the domain size. The preferential vertical clustering as found in the experiments by Martínez Mercado et al. (2010) was not observed in the numerical results. We attribute this to the lack of large-scale flow circulations due to the limited size of the computational domain and absence of walls in the domain. Instead, strong diagonal clustering effects are observed. More simulations using larger domains *with* walls will be required to further elucidate this issue. The domain size (and the closely related number of bubbles) and boundary conditions are very important for the spatial orientation of the bubbles, whereas the influence of these parameters is of less importance for the energy spectra calculations.

Acknowledgments

This work is part of the industrial partnership programme: *Fundamentals of heterogenous bubbly flows* of the Foundation for Fundamental Research on Matter (FOM), which is financially supported by the Dutch Organization for Scientific Research (NWO) and the industrial partners AkzoNobel, DSM, Shell and Tata Steel of the IPP-FOM programme.

References

Bunner, B., Tryggvason, G., 2002a. Dynamics of homogeneous bubbly flows part 1. Rise velocity and microstructure of the bubbles. J. Fluid Mech. 466, 17–52.
Bunner, B., Tryggvason, G., 2002b. Dynamics of homogeneous bubbly flows part 2. Velocity fluctuations. J. Fluid Mech. 466, 53–84.
Bunner, B., Tryggvason, G., 2003. Effect of bubble deformation on the properties of bubbly flows. J. Fluid Mech. 495, 77–118.
Calzavarini, E., Doering, C.R., Gibbon, J.D., Lohse, D., Tanabe, A., Toschi, F., 2006. Exponentially growing solutions in homogeneous Rayleigh–Bénard convection. Phys. Rev. E 73, 035301.
Deen, N., Van Sint Annaland, M., Kuipers, J., 2004. Multi-scale modeling of dispersed gas-liquid two-phase flow. Chem. Eng. Sci. 59, 1853–1861.

Dijkhuizen, W., Roghair, I., Van Sint Annaland, M., Kuipers, J., 2010a. DNS of gas bubbles behaviour using an improved 3D front tracking model–drag force on isolated bubbles and comparison with experiments. Chem. Eng. Sci. 65, 1415–1426.

Dijkhuizen, W., Roghair, I., Van Sint Annaland, M., Kuipers, J., 2010b. DNS of gas bubbles behaviour using an improved 3D front tracking model–model development. Chem. Eng. Sci. 65, 1427–1437.

Esmaeeli, A., Tryggvason, G., 2005. A direct numerical simulation study of the buoyant rise of bubbles at O(100) Reynolds number. Phys. Fluids 17, 093303.

Lance, M., Bataille, J., 1991. Turbulence in the liquid phase of a uniform bubbly air–water flow. J. Fluid Mech. 222, 95–118.

Martínez Mercado, J., Chehata Gómez, D., van Gils, D., Sun, C., Lohse, D., 2010. On bubble clustering and energy spectra in pseudo-turbulence. J. Fluid Mech. 650, 287–306.

Martínez Mercado, J., Palacios Morales, C., Zenit, R., 2007. Measurements of pseudoturbulence intensity in monodispersed bubbly liquids for $10 < Re < 500$. Phys. Fluids 19, 103302.

Mazzitelli, I., Lohse, D., 2009. Evolution of energy in flow driven by rising bubbles. Phys. Rev. E 79, 066317.

Mudde, R., Groen, J., van der Akker, H., 1997. Liquid velocity field in a bubble column: LDA experiments. Chem. Eng. Sci. 52, 4217.

Riboux, G., Risso, F., Legendre, D., 2010. Experimental characterization of the agitation generated by bubbles rising at high Reynolds number. J. Fluid Mech. 643, 509–539.

Risso, F., 2011. Theoretical model for k^{-3} spectra in dispersed multiphase flows. Phys. Fluids 23, 011701.

Risso, F., Ellingsen, K., 2002. Velocity fluctuations in a homogeneous dilute dispersion of high-Reynolds-number rising bubbles. J. Fluid Mech. 453, 395–410.

Risso, F., Roig, V., Amoura, Z., Riboux, G., Billet, A., 2008. Wake attenuation in large Reynolds number dispersed two-phase flows. Philos. Trans. Roy. Soc. A 366, 2177–2190.

Roig, V., de Tournemine, L., 2007. Measurement of interstitial velocity of homogeneous bubbly flows at low to moderate void fraction. J. Fluid Mech. 572, 87–110.

Tryggvason, G., Bunner, B., Esmaeeli, A., Juric, D., Al-Rawahi, N., Tauber, W., Han, J., Nas, S., Jan, Y., 2001. A front-tracking method for the computations of multiphase flow. J. Comput. Phys. 169, 708–759.

Unverdi, S., Tryggvason, G., 1992. A front-tracking method for viscous, incompressible, multi-fluid flows. J. Comput. Phys. 100, 25–37.

van den Berg, T., Wormgoor, W.D., Luther, S., Lohse, D., 2011. Phase-sensitive constant temperature anemometry. Macromol. Mater. Eng., 296.

van Sint Annaland, M., Dijkhuizen, W., Deen, N., Kuipers, J., 2006. Numerical simulation of behavior of gas bubbles using a 3-D front-tracking method. AIChE J. 52, 99–110.

Zenit, R., Koch, D., Sangani, A., 2001. Measurements of the average properties of a suspension of bubbles rising in a vertical channel. J. Fluid Mech. 429, 30–342.